Journal of Solid State Chemistry **162,** 379–388 (2001)
doi:10.1006/jssc.2001.9328, available online at http://www.idealibrary.com on IDEAL®

Crystal Structure of $La_{24}Li_{20}Ti_5O_{56}$: A Pseudo-Close-Packed, Columnar Intergrowth Stucture

Caroline A. Kirk and Anthony R. West[1]

Department of Engineering Materials, University of Sheffield, Mappin Street, Sheffield, S1 3JD, United Kingdom

IN HONOR OF PROFESSOR PAUL HAGENMULLER ON THE OCCASION OF HIS 80TH BIRTHDAY

The crystal structure of $La_{24}Li_{20}Ti_5O_{56}$ has been solved by a combination of selected area electron diffraction (SAED) and powder X-ray and neutron diffraction. The structure has a strong tetragonal subcell a = 13.244(1) Å, c = 7.463(1) Å, space group *P4/mbm* (127); by SAED, a weak supercell with doubled c is observed. The subcell structure contains alternating columns of (i) perovskite-like structure, with Li, Ti in alternating octahedral sites, and (ii) a more complex structure that is distantly related to fluorite; one half of the tetrahedral sites in fluorite is occupied in pairs by Li, but the other half of the pairs of tetrahedral sites collapse to contain either a single octahedral site occupied by Ti, or a single tetrahedral site occupied by Li. The Li sites that form the edge-sharing pairs are not fully occupied. Possible ordering of Li/vacancies within these sites may be responsible for the superstructures seen by SAED. The structure is not close-packed, *cp*, overall but the *cp* arrangements of O and La within the columns give the structure a high packing density. © 2001 Elsevier Science

INTRODUCTION

The Li_2O–La_2O_3–TiO_2 system contains a perovskite-related phase, $Li_{1/2-3x}La_{1/2+x}TiO_3$, $0.02 < x < 0.13$, which exhibits exceptionally high levels of lithium ion conductivity, σ (1,2). Composition $x \sim 0.07$ has $\sigma = 1.1 \times 10^{-3}$ $\Omega^{-1}\,cm^{-1}$ at 25°C, which is the highest yet found for Li^+ ion conduction in any stable oxide system. During a study of compound formation and ionic conductivity in the system Li_2O–La_2O_3–TiO_2 (3), we encountered the new phase $La_{24}Li_{20}Ti_5O_{56}$. At the outset its composition, especially its Li content, was known only approximately due to Li volatilization during high-temperature synthesis. Since single crystals were unavailable, its structure determination required the use of three diffraction techniques: selected area electron diffraction, SAED, to determine the unit cell and possible space group(s); powder X-ray diffraction, XRD, to locate the La positions, using direct methods; and combined XRD and powder neutron diffraction, ND, to locate the remaining atoms using a modified Rietveld approach combined with difference Fourier analysis, DFA. For the final stages, bond valence analysis, BVA, and calculation of the charge imbalance around various oxygen positions enabled Li atoms to be located. A preliminary report of the structure of this new phase has been published (4); due to the unique nature of its columnar intergrowth structure and the complex strategy required to solve the structure, a more complete description is given here.

EXPERIMENTAL

Starting materials Li_2CO_3, La_2O_3, and TiO_2 were dried at 200, 1000, and 600°C, respectively, and stored in a desiccator. Reaction mixtures were prepared in 5–10-g amounts; reagents were weighed out, ground together in an agate mortar under acetone, dried, and fired in Au foil boats, initially at 650–700°C for a few hours to expel CO_2 and initiate reaction. After various trial-and-error studies, during which it was realized that volatilization of Li_2O occurred on heating mixtures at ~800–950°C, the following procedure was adopted. The prefired powders were divided into three portions, two of which were cold-pressed uniaxially to form pellets; the pellets were stacked in a gold boat and covered with the remaining powder. The assembly was then fired at 900°C for 12 h to complete reaction; using this method, the lower pellet, which was surrounded by a Li_2O-rich environment, appeared to suffer less lithia loss than the covering powder. Nevertheless, the stoichiometry obtained by subsequent structure refinement showed that significant amounts of lithia loss had still occurred.

Products were analyzed by powder XRD using a Stoe StadiP diffractometer with a small, linear position-sensitive detector and Cu$K\alpha_1$ radiation. For structural studies, data were collected over the 2θ range $8° < 2\theta < 120°$, with a detector step width of 0.1° and data collection time of 14 h. For SAED, a JEOL Temscan 2000EX was used. ND data were collected at the UK spallation source ISIS, Rutherford Appleton Laboratory, on the POLARIS instrument, from

[1]To whom correspondence should be addressed.

0022-4596/01 $35.00

the highest resolution detectors, over the time-of-flight range 2000–19,500 μs.

RESULTS

During the phase diagram study on the Li_2O–La_2O_3–TiO_2 system (3), characteristic XRD lines of a new phase, initially labelled as phase C, were seen in a variety of compositions, usually in combination with various other lithium and/or lanthanum titanate phases, or unreacted La_2O_3. Gradually, a target composition of this new phase was obtained as $7La_2O_3.10Li_2O.3TiO_2$ or $La_{14}Li_{20}Ti_3O_{37}$, which was essentially phase-pure by XRD. A large sample of this composition was therefore prepared for structural studies. It was not possible to establish its unit cell dimensions and space group by trial-and-error indexing of its powder XRD pattern; the next step was therefore to use SAED.

Selected Area Electron Diffraction

Initially, a survey was carried out of the SAED patterns of a number of crystallites, some of which were tilted about prominent axes in the SAED patterns; these were used to build up a picture of the reciprocal lattice. A set of diffraction patterns, typical for most of the crystals examined, is shown in Figs. 1a–1c. The section shown in Fig. 1a, which has square symmetry with $\mathbf{a} = 13.24$ Å, was labelled $\mathbf{a}^*\mathbf{a}^*$. On tilting around $\mathbf{a}^*$, different Laue zones were observed, from which a centered rectangular section was constructed. By examining crystals that were oriented differently, the SAED pattern in Fig. 1b was found, which matched the rectangular section constructed by tilting around $\mathbf{a}^*$. This indicated the crystal system to be tetragonal, $\mathbf{a} = 13.24$ Å and $\mathbf{c} = 15.0$ Å.

The next step was to index the SAED patterns to determine a possible space group(s). The $\mathbf{a}^*\mathbf{a}^*$ pattern, Fig. 1a,

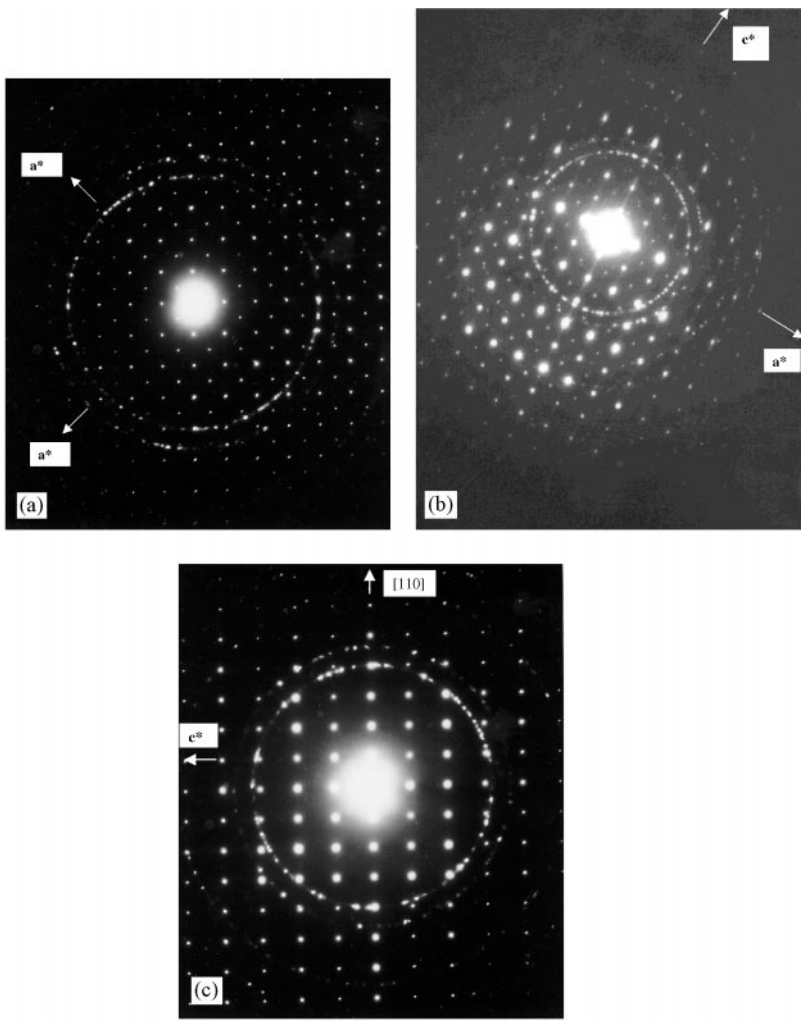

FIG. 1. (a) $\mathbf{a}^*\mathbf{a}^*$ section, (b) $\mathbf{a}^*\mathbf{c}^*$ section, and (c) $\mathbf{a}^*$ [110] sections through the reciprocal lattice.

has no extinction conditions; however, the $0k0$ reflections, where $k = 2n$, are all noticeably more intense than those where $k = 2n + 1$. When the crystals were tilted around **a***, these intensity variations became more pronounced and the reflections, $k = 2n + 1$, were no longer present at high tilt angles. The reflections where $0k0$, $k = 2n + 1$, are completely absent from Fig. 1b; this section is at 90 to the 001 zone, Fig. 1a. From this it was proposed that the condition for reflection, $0k0$, $k = 2n$, holds and that the extra reflections are spurious. They may arise due to either multiple diffraction or, because of the large **a** parameter and the relative thinness of the crystals, they may be parts of elongated reflections that actually belong to higher order zones.

The **a***c*, Fig. 1b, section was then indexed and the condition for reflection, $0kl$, $k + l = 2n$, was found. From other sections of the reciprocal lattice, the condition for reflection, hhl, $l = 2n$, was also observed, Fig. 1c. Therefore, the conditions for reflection were $0kl$, $k + l = 2n$, hhl, $l = 2n$, and the possible space groups matching these conditions for reflection are $P4/mnc$ (128) or $P4nc$ (104).

In addition to the sharp diffraction patterns referred to above, some crystals showed streaking through the subcell reflections with streaking parallel to **c***. Origins of this are unknown but are possibly related to either small domain size or stacking disorder in the **c** direction.

Powder X-Ray Diffraction

Using the unit cell dimensions determined by SAED as a starting point, the XRD pattern was indexed as primitive tetragonal with refined dimensions, **a** = 13.2443 (13) Å and **c** = 14.9258 (20) Å. Inspection of the indexing showed that for all observed reflections, $l = 2n$. The XRD pattern can therefore be re-indexed on a smaller unit cell with halved **c**, i.e., **a** = 13.2443(13) Å and **c** = 7.4629(10) Å, Table 1. Thus, the doubled **c** axis obtained by SAED is not detected by XRD.

TABLE 1
Indexed XRD Powder Pattern of $La_{24}Li_{20}Ti_5O_{56}$

h	k	l	$\Delta 2\theta$ obs-calc	Int.	$d_{(obs)}$ (Å)	$d_{(calc)}$ (Å)
1	1	0	−0.0181	51.8	9.3831	9.3651
2	0	0	−0.0135	25.7	6.6288	6.6221
2	2	0	0.0142	11.3	4.6791	4.6825
3	1	0	0.0027	7.1	4.1877	4.1882
0	0	2	−0.0157	6.8	3.7339	3.7314
1	1	2	−0.0027	17.7	3.4668	3.4664
4	0	0	0.0000	49.2	3.3111	3.3111
2	0	2	−0.0043	35.3	3.2514	3.2509
4	1	0	−0.0121	8.3	3.2136	3.2122
3	3	0	−0.0073	42.8	3.1225	3.1217
4	2	0	0.0137	41.0	2.9602	2.9615
2	2	2	−0.0003	100.0	2.9182	2.9182
3	1	2	−0.0019	10.1	2.7862	2.7861
5	1	0	0.0013	18.6	2.5973	2.5974
3	3	2	0.0053	47.1	2.3940	2.3943
4	4	0	0.0031	18.1	2.3411	2.3413
4	2	2	0.0014	8.7	2.3196	2.3197
5	3	0	−0.0026	6.5	2.2715	2.2714
6	0	0	0.0031	5.1	2.2072	2.2074

Structure Determination

At the outset, the structure and composition of phase C were unknown. A search using the ICSD database found a possible analogue, $La_{24}Li_{22}Fe_6O_{56}$, with **a** = 13.240 Å, **c** = 7.497 Å and space group $P4/mbm$ (127) (5). The refined unit cell parameters of phase C are very close to those for $La_{24}Li_{22}Fe_6O_{56}$. The stoichiometry of $La_{24}Li_{22}Fe_6O_{56}$ is, however, different from that originally proposed for phase C, $La_{14}Li_{20}Ti_3O_{37}$. Further, although the composition, $La_{14}Li_{20}Ti_3O_{37}$, was phase-pure by XRD, a second phase, Li_4TiO_4, was detected by ND. The La:Ti ratio of the initial stoichiometry (4.667:1) is fairly close to the La:Fe ratio of $La_{24}Li_{22}Fe_6O_{56}$ (4:1) and taking into account the probable loss of lithia, it seemed likely that the Li and O contents of composition $La_{14}Li_{20}Ti_3O_{37}$ are incorrect. Rietveld refinement of XRD and ND data for phase C was attempted, assuming that it had a formula and structure similar to those of $La_{24}Li_{22}Fe_6O_{56}$ with Fe replaced by Ti and all sites fully occupied.

Full Rietveld refinement of neither the XRD nor the ND data was possible. The refinements did not converge satisfactorily and the resulting model contained some unreasonably short bond lengths. It was therefore necessary to attempt a structure solution by *ab initio* methods. At the conclusion of the structure determination, comparison with the structural parameters for $La_{24}Li_{22}Fe_6O_{56}$ indicated a probable error in the coordinates of one oxygen position, O(2), which was why this model could not be used.

The first step used the direct methods program SIRPOW (6) on the XRD dataset to locate the heavy atoms. The three peaks of highest electron density, attributed to La, had coordinates 0.006, 0.96, 0.25; 0.26, 0.76, 0; and 0.22, 0.72, 0.5. These positions were used as a starting point for partial Rietveld refinement of combined XRD and ND data using the Rietveld program GSAS (7). Difference Fourier analysis (DFA) was then carried out and possible sites for Ti and O atoms were located. The process involved adding one or two atoms to the partial model, followed by Rietveld refinement and then DFA to locate more atoms. After several cycles, the partial structure given in Table 5[2] resulted in the formula $La_{24}Ti_6O_{48}$.

At this stage it was difficult to locate any more atoms by DFA of the XRD or ND datasets. Although the formula "$La_{24}Ti_6O_{48}$" had charge balance, no Li had been located and any extra positive charge would require extra O atoms.

[2]The approximate atomic coordinates and atom labels can be inferred from the final listing, Table 2.

The coordination of the cations in the partial structure was six-fold for La(2) and La(3) and four-fold for Ti(4), which is rare, although not unknown (8, 9). A projection of Ti(4) and its surroundings showed that an O site, O(13), with coordinates 0.214, 0.714, 0.183, mirroring those of O(9), would give octahedral coordination for Ti(4). Rietveld refinement incorporating O(13) converged satisfactorily giving reasonable Ti(4)–O and La(2)–O(13) bond lengths.

In order to locate Li, BVA was used to check gross departures from electroneutrality. This showed convincingly that the La and Ti(4) sites are essentially full but Ti(12) had a BV sum of only 3.09, which could indicate either Ti vacancies or occupancy by a mixture of Ti and Li. The amount of positive charge around the O atoms was also calculated; O(5), O(6), O(8), O(9), and O(10) were found to be particularly underbonded.

A possible Li site at 0, 0, 0.5 coordinated to O(6) (×4) and O(8) (×2), was identified which would give chains of corner-sharing TiO_6/LiO_6 octahedra running parallel to **c**. Li(14) was therefore added to the refinement but the thermal parameters of both Li(14) and Ti(12) were unstable and the refinement diverged. The possibility of Li/Ti disorder over the Ti(12) and Li(14) sites was tested, constraining the total occupancy of each site to be one. Refinement indicated mixed Ti/Li occupancy for Ti(12) but Li occupancy only of Li(14). Possible Li sites, Li(15), situated between two O(5) atoms with approximate coordinates 0.084, 0.584, 0.25 and Li(16) bonded to O(9) and O(10), at 0.09, 0.41, 0.186, were identified. Rietveld refinement incorporating Li(15) and Li(16) was carried out and convergence achieved. A possible octahedral site for Li, Li(17) at 0.097, 0.403, $\frac{1}{2}$, was identified, but on refinement, it displaced into an adjacent distorted tetrahedral site at 0.121, 0.378, $\frac{1}{2}$.

At this stage, bond length calculations showed distorted Ti(12) and Li(14) octahedra, with four long equatorial Ti–O bonds, ~2.25 Å, and two short axial bonds, ~1.8 Å. To equalize bond lengths, Ti could be displaced either between two Ti–O bonds in the xy plane or between three Ti–O bonds out of the *xy* plane. Refinement of the first possibility converged with a small off-center displacement in the *xy* plane giving slightly improved bond lengths but negative thermal parameters. At the conclusion of the structure determination, the possibility of off-center displacements was re-investigated, but it was concluded that, within errors, such displacements could not be confirmed.

The stoichiometry at this stage, assuming full occupancy of Ti(12) by Ti, was $La_{24}Li_{20}Ti_6O_{56}$, which is still either deficient by two oxygens or has an effective excess cation charge of 4 + . The DFA maps had no residual peaks which could be associated with missing oxygen atoms. Therefore, the amount of positive charge must be decreased, by either introducing vacancies onto the La, Ti, Li sites or altering the amounts of Ti and Li on the mixed (Ti/Li) sites. From the U_{iso} values, there was no evidence for vacancies on the La and Ti(4) sites. The Ti(12) site refined well with a 50:50 occupancy by Ti and Li. Li(14) and Li(17) appeared to be full; Li(15) and Li(16) showed evidence of partial occupancy and, to achieve charge balance, their occupancy was fixed at 0.8125.

The final refinement was based on the stoichiometry $La_{24}Li_{20}Ti_5O_{56}$; all parameters, including U_{iso}'s, were refined simultaneously using combined XRD and ND datasets and satisfactory convergence obtained. Final coordinates are given in Table 2 with bond lengths and

TABLE 2
Refined Atomic Positions and Thermal Parameters of $La_{24}Li_{20}Ti_5O_{56}$

Atom	*x*	*y*	*z*	U_{iso} (Å^2)	Occ.	Wyckoff
La(1)	0.00891(14)	0.19610(9)	0.25695(29)	0.01879(24)	1.0	16*l*
La(2)	0.26120(15)	0.76120(15)	0	0.01137(49)	1.0	4*g*
La(3)	0.21899(15)	0.71899(15)	0.5	0.01018(47)	1.0	4*h*
Ti(4)	0.08561(34)	0.58561(34)	0	0.01269(12)	1.0	4*g*
O(5)	0.32056(23)	0.01785(23)	0.5	0.01335(50)	1.0	8*j*
O(6)	0.12283(24)	0.11807(28)	0.5	0.01314(52)	1.0	8*j*
O(7)	0.12357(32)	0.11299(33)	0	0.02769(86)	1.0	8*i*
O(8)	0	0	0.25287(78)	0.01654(59)	1.0	4*e*
O(9)	0	0.5	0.18485(51)	0.01281(65)	1.0	4*f*
O(10)	0.18469(17)	0.31531(17)	0.28879(45)	0.01841(64)	1.0	8*k*
O(11)	0.02838(28)	0.31350(29)	0	0.02308(65)	1.0	8*i*
Ti/Li(12)	0	0	0	0.01595(263)	0.5/0.5	2*a*
O(13)	0.15598(19)	0.65598(19)	0.18965(52)	0.02787(66)	1.0	8*k*
Li(14)	0	0	0.5	0.01096(294)	1.0	2*b*
Li(15)	0.07629(48)	0.57629(48)	0.34381(115)	0.00661(136)	0.8125	8*k*
Li(16)	0.09743(50)	0.40257(50)	0.16817(117)	0.00839(138)	0.8125	8*k*
Li(17)	0.12107(51)	0.37893(51)	0.5	0.00787(177)	1.0	4*h*

Note. $\chi^2 = 5.393$, $wRp_{overall} = 3.62\%$, $Rp_{overall} = 4.86\%$. Number of observables (N) = 9540, number of refined parameters (P) = 39, number of constraints (C) = 1.

TABLE 3
Bond Lengths and Bond Angles of $La_{24}Li_{20}Ti_5O_{56}$

Atoms	Bond length (Å)	Atoms	Bond Length (Å)
La(1)–O(5)	2.478(3)	La(2)–O(7)	2.488(4)×2
La(1)–O(6)	2.578(3)	La(2)–O(10)	2.383(3)×2
La(1)–O(6)	2.659(3)	La(2)–O(11)	2.874(4)×2
La(1)–O(7)	2.684(4)	La(2)–O(13)	2.428(4)×2
La(1)–O(7)	2.684(4)		
La(1)–O(8)	2.602(1)	La(3)–O(5)	2.717(4)×2
La(1)–O(10)	2.825(2)	La(3)–O(6)	2.487(4)×2
La(1)–O(11)	2.484(3)	La(3)–O(10)	2.398(4)×2
La(1)–O(13)	2.979(2)	La(13)–O(13)	2.601(4)×2
Ti(4)–O(9)	2.117(5)×2	Ti/Li(12)–O(7)	2.219(4)×4
Ti(4)–O(11)	2.018(4)×2	Ti/Li(12)–O(8)	1.888(6)×2
Ti(4)–O(13)	1.935(6)×2		
		Li(14)–O(6)	2.258(4)×4
Li(15)–O(5)	1.957(6)×2	Li(14)–O(8)	1.845(6)×2
Li(15)–O(9)	1.859(10)		
Li(15)–O(13)	1.886(9)×2	Li(16)–O(9)	1.831(9)
		Li(16)–O(10)	1.867(10)
Li(17)–O(5)	1.997(5)×2	Li(16)–O(11)	1.954(6)×2
Li(17)–O(10)	1.977(5)×2		
O(9)–Ti(4)–O(9)	80.06(27)	O(7)–Ti/Li(12)–O(7)	90×4
O(9)–Ti(4)–O(11)	86.95(18)×4	O(7)–Ti/Li(12)–O(7)	180×2
O(9)–Ti(4)–O(13)	92.35(14)×2	O(8)–Ti/Li(12)–O(7)	90×8
O(9)–Ti(4)–O(13)	172.42(28)×2	O(8)–Ti(12)/Li–O(8)	180
O(11)–Ti(4)–O(11)	172.0(5)		
O(11)–Ti(4)–O(13)	92.68(15)×4	O(6)–Li(14)–O(6)	90×4
O(13)–Ti(4)–O(13)	95.2(4)	O(6)–Li(14)–O(6)	180×2
		O(8)–Li(14)–O(6)	90×8
		O(8)–Li(14)–O(8)	180
O(5)–Li(15)–O(5)	102.2(4)		
O(5)–Li(15)–O(9)	124.54(28)×2	O(9)–Li(16)–O(9)	147.4(5)
O(5)–Li(15)–O(13)	99.23(34)×2	O(9)–Li(16)–O(11)	97.59(34)
O(9)–Li(15)–O(13)	100.7(4)	O(10)–Li(16)–O(11)	103.4(4)
		O(11)–Li(16)–O(11)	98.9(4)
O(5)–Li(17)–O(10)	103.13(10)×2		
O(10)–Li(17)–O(10)	105.6(5)		
O(5)–Li(17)–O(5)	180		

angles in Table 3. Difference profiles of the ND and XRD datasets are given in Fig. 2a and 2b, respectively. The first set of tic marks present on the ND profiles show the reflection positions of the impurity phase Li_4TiO_4. A comparison of the goodness-of-fit parameter χ^2 and R values of the partial structure $La_{24}Ti_6O_{48}$ with those of $La_{24}Li_{20}Ti_5O_{56}$ is given in Table 4, showing a clear improvement in the fit when the extra O and Li sites are added.

The final refined stoichiometry, $La_{24}Li_{20}Ti_5O_{56}$, is different from that of the starting material, $La_{28}Li_{40}Ti_6O_{74}$, as it has much less Li. The La:Ti ratios are approximately the same, however, and it is highly likely that lithia loss occurred during synthesis, despite the precautions taken.

Description of the Structure

The structure of $La_{24}Li_{20}Ti_5O_{56}$ is complex and cannot be described in terms of any simple known structure type. The structure is not close-packed since only one atom, O(8), is 12-coordinate. All other O and La atoms have lower coordination numbers.

Figure 3 shows the **ac** projection of the La and O atoms only. Mixed layers of La and O occur perpendicular to **c**, which are alternately buckled and planar. Figure 4 represents **ab** sections at different **c** heights, corresponding to the two layer types at $z = 0$, 0.5 (flat), Figs. 4a and 4c, and $z \sim 0.25$, 0.75 (buckled), Fig. 4b.

The section, Fig. 4b, at $z \sim 0.25$ has two sets of domino five-like patterns, rotated by 45 with respect to each other. If this section is idealized, so that all atoms lie at $z = 0.25$, and O–O, La–O distances are equalized, the projection shown in Fig. 5a is obtained. One domino five set has O(8) centered at the corner and at the **ab** face center, surrounded by four La(1) atoms (white square). The other set centered on O(9) at the edge center positions is surrounded by four oxygens O(10) and O(13) (black square).

The sections at $z = 0$ and $z = 0.5$ are very similar, Fig. 5b. The squares centered at the corner and the center of the **ab** face (outlined in white) lie directly above and below the O(8) domino five pattern at $z = 0.25$, and effectively lead to infinite columns of face-centred cubes, *fcc*, parallel to **c**. Within the columns, the La:O ratio is 1:3 and their arrangement is as in perovskite. The sites for Ti and Li (at 0, 0, 0 and 0, 0, 0.5) are also the same as in perovskites and, therefore, perovskite-like columns may be identified, Fig. 6a, with a repeat unit of two perovskite subcells along **c**.

The second set of domino five-like patterns, Fig. 5a outlined in black, also form part of distorted *fcc* columns parallel to **c**, by alternating with squares of O atoms, above and below, at $z = 0$ and $z = 0.5$, Fig. 5b. Within these columns, Li(15) and Li(16) occupy half the tetrahedral sites in such a way that half of the structure is fluorite-related, by forming edge-sharing pairs along **c**, Figs. 6b, 6c, and 7. However, the other half of the pairs of tetrahedral sites (that would be occupied in fluorite) collapse into either a single occupied tetrahedral site Li(17), Figs. 6c and 7, or a single occupied octahedral site Ti(4), Figs. 6b and 7. The octahedral site formed by collapsing an edge-sharing pair of tetrahedra (at $z \sim 0.125$ and $z \sim 0.875$) onto an octahedral site at $z = 0$ causes O(11) to move toward the Ti site in the **ab** plane and O(9), O(13) to move from $z = 0.25$ toward the basal plane. This rearrangement of O sites causes the puckering of layers at $z \sim 0.25$ and $z \sim 0.75$.

The distorted *fcc* columns, Fig. 7, consist of four quarter columns which occur in pairs. In one pair, the edge-sharing sequence, $Ti(4)O_6$, $Li(15)O_4$, $Li(15)O_4$, occurs parallel to **c**, Fig. 6b, and TiO_6 octahedra in adjacent quarter-columns share edges, formed by oxygens O(9). In the other pair, edge-sharing pairs of $Li(16)O_4$ tetrahedra corner-share with $Li(17)O_4$ tetrahedra parallel to **c**, Fig. 6c.

Thus far, two idealized structural components have been identified, perovskite columns and more complex columns,

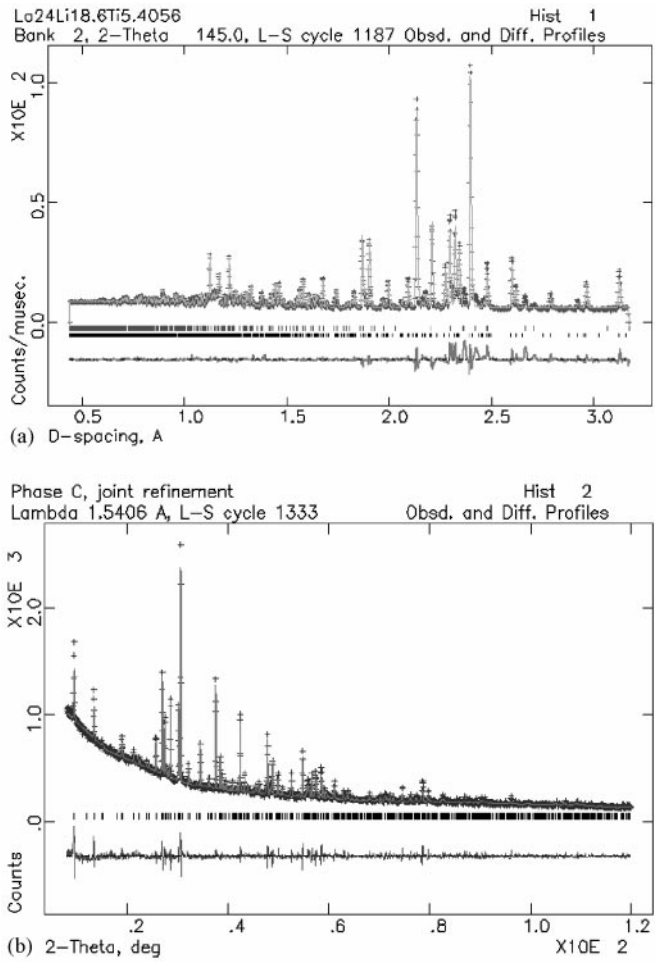

FIG. 2. Observed, calculated, and difference plots of (a) ND and (b) XRD datasets. In (a) the positions of the reflections of impurity phase Li_4TiO_4 are the first set of tic marks.

distantly related to fluorite. The latter set of columns were described in (4) as distantly related to twinned zinc blende. Since that preliminary report, the Li(17) positions have been located; neither these positions nor those of Ti(4) are occupied in either zinc blende or fluorite. However, the edge-sharing pairs of Li(15) and Li(16) tetrahedra occupy the same positions as in fluorite but need to be twinned to show a relationship to zinc blende. For this reason we prefer to describe the columns as being related to fluorite.

The two sets of columns, perovskite- and fluorite-related, are connected, through La(2) and La(3) to form the 3D structure of $La_{24}Li_{20}Ti_5O_{56}$, Fig. 8. The perovskite-type columns are regular, whereas the fluorite-related columns are very distorted.

TABLE 4
Comparison of χ^2 and R Values

	$La_{24}Ti_6O_{48}$	$La_{24}Li_{20}Ti_5O_{56}$
χ^2	16.31	5.393
wRp$_{ND}$	6.28	3.43
Rp$_{ND}$	11.61	6.39
wRp$_{XRD}$	6.83	6.46
Rp$_{XRD}$	4.91	4.73
wRp$_{overall}$	6.30	3.62
Rp$_{overall}$	5.44	4.86

TABLE 5
Refined Atomic Positions and U_{iso} of the Partial Structure "$La_{24}Ti_6O_{48}$"

Atom	x	y	z	U_{iso} (Å^2)	Occ.	Wyckoff
La(1)	0.01023	0.19502	0.25404	0.0197	1.0	16*l*
La(2)	0.26193	0.76193	0	0.0099	1.0	4*g*
La(3)	0.21906	0.71906	0.5	0.0099	1.0	4*h*
Ti(4)	0.10820	0.60820	0	0.0167	1.0	4*g*
O(5)	0.32081	0.01646	0.5	0.0137	1.0	8*j*
O(6)	0.12378	0.11941	0.5	0.0191	1.0	8*j*
O(7)	0.12361	0.11126	0	0.0191	1.0	8*i*
O(8)	0	0	0.24924	0.0143	1.0	4*e*
O(9)	0	0.5	0.18375	0.0140	1.0	4*f*
O(10)	0.17901	0.32099	0.29431	0.0167	1.0	8*k*
O(11)	0.02951	0.31738	0	0.0261	1.0	8*i*
Ti(12)	0	0	0	0.0071	1.0	2*a*

Comparison of $La_{24}Li_{20}Ti_5O_{56}$ with $La_{24}Li_{22}Fe_6O_{56}$

The stoichiometries of $La_{24}Li_{22}Fe_6O_{56}$ and $La_{24}Li_{20}Ti_5O_{56}$ are very similar. Comparison of the final refined parameters for $La_{24}Li_{20}Ti_5O_{56}$, Table 2, with those of $La_{24}Li_{22}Fe_6O_{56}$ (5) showed that three La and most O positions are the same in both. However, O(2) in $La_{24}Li_{22}Fe_6O_{56}$ is not part of the structure of $La_{24}Li_{20}Ti_5O_{56}$, and conversely, O(6) in $La_{24}Li_{20}Ti_5O_{56}$ is not part of $La_{24}Li_{22}Fe_6O_{56}$. Consequently, the site 0, 0, 0.5 which is proposed to contain octahedral Li in $La_{24}Li_{22}Fe_6O_{56}$ but is only two-coordinate, is octahedrally coordinated in $La_{24}Li_{20}Ti_5O_{56}$. The latter has Ti and Li disordered over Ti(12), but $La_{24}Li_{22}Fe_6O_{56}$ has Fe on this site.

Bond valence sums calculated using the parameters from $La_{24}Li_{22}Fe_6O_{56}$ indicated underbonding of La(1), La(3), and Li(1) and overbonding of Li(15) and Li(18) It appears, therefore, that the reported structure of $La_{24}Fe_6Li_{22}O_{56}$ is incorrect in detail and instead, its structure may be analogous to that of $La_{24}Li_{20}Ti_5O_{56}$, especially since the stoichiometries of the two phases are so similar. In particular, it appears that there may be an error in one of the oxygen coordinates: O(6) is listed as 0.03823, 0.3773, $\frac{1}{2}$, whereas it should probably be closer to 0.03832, 0.03773, $\frac{1}{2}$.

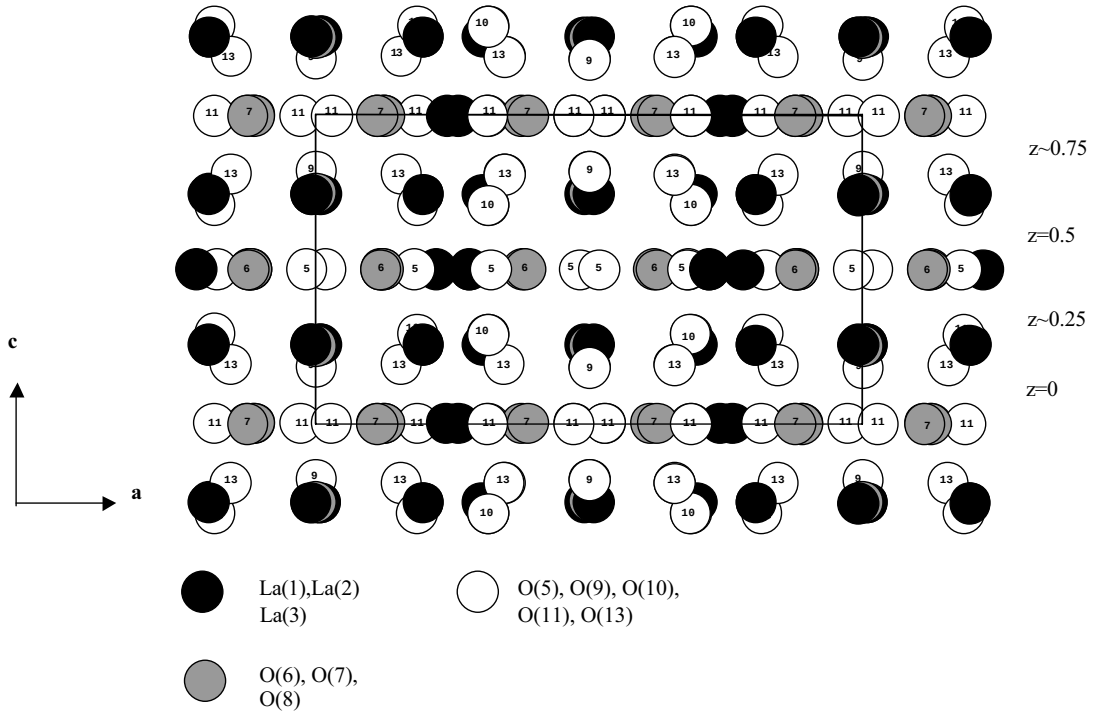

FIG. 3. **ac** projection, showing flat and buckled La, O layers perpendicular to **c**.

CONCLUSIONS

$La_{24}Li_{20}Ti_5O_{56}$ has a tetragonal subcell with $\mathbf{a} = 13.2443(13)$ Å, $\mathbf{c} = 7.4692(10)$ Å and space group *P*4/*mbm*. SAED data suggest a doubling of **c**, introducing reflection conditions associated with either of the space groups *P*4*nc* (104) and *P*4/*mnc* (128). Structure determination and refinement of the XRD and ND data were carried out in the smaller unit cell with space group *P*4/*mbm*. There was no evidence from either the XRD or ND datasets for the presence of superlattice reflections that would require a doubling of **c**.

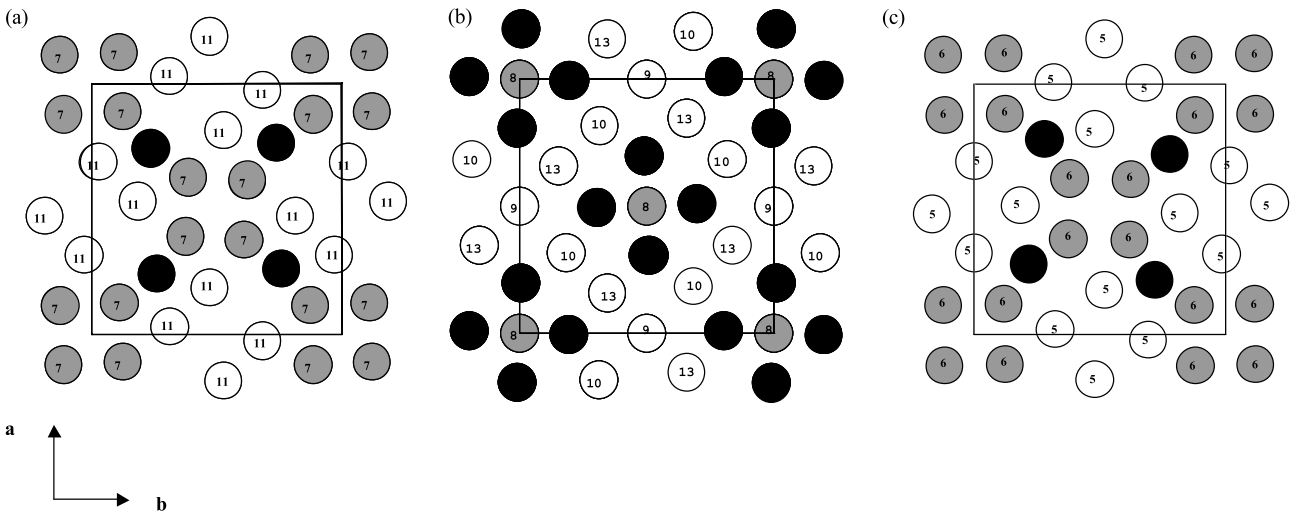

FIG. 4. **ab** sections showing La, O layers at (a) $z = 0$, (b) $z = 0.25$ and 0.75, and (c) $z = 0.5$.

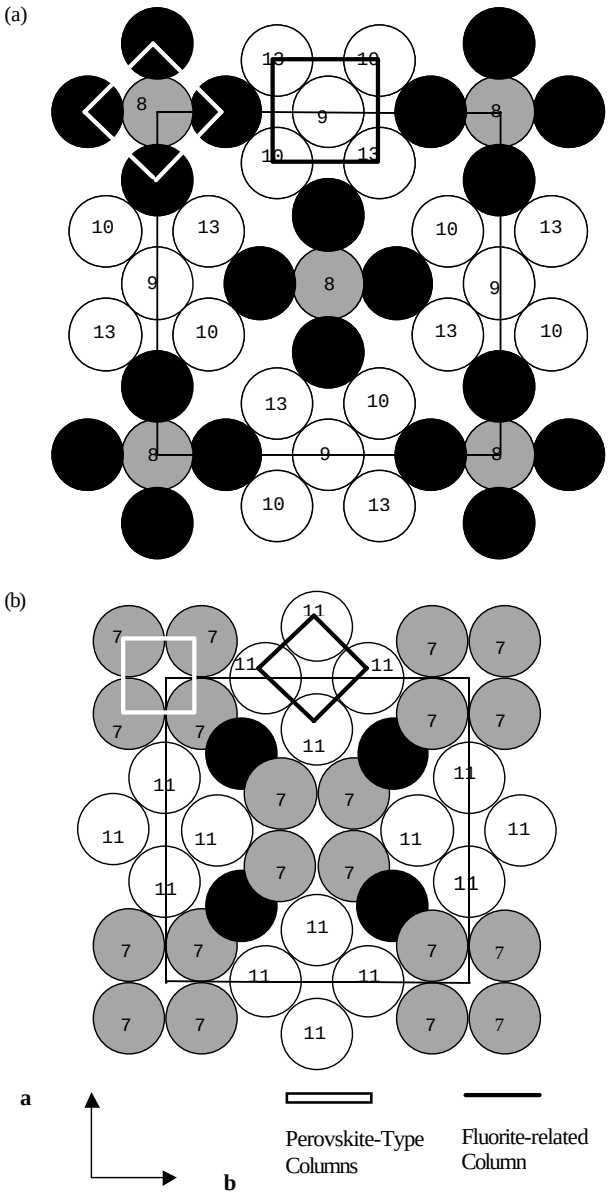

FIG. 5. Idealized sections at (a) $z = 0.25$ and (b) $z = 0$.

There are several possible explanations for the doubling observed by SAED. First, it may be due to ordering of the Li and Ti atoms, which are disordered over the Ti(12) sites; given the relatively strong scattering power of Ti by X rays, this should be apparent in the XRD data and is therefore unlikely to be the explanation. Second, tilting of the

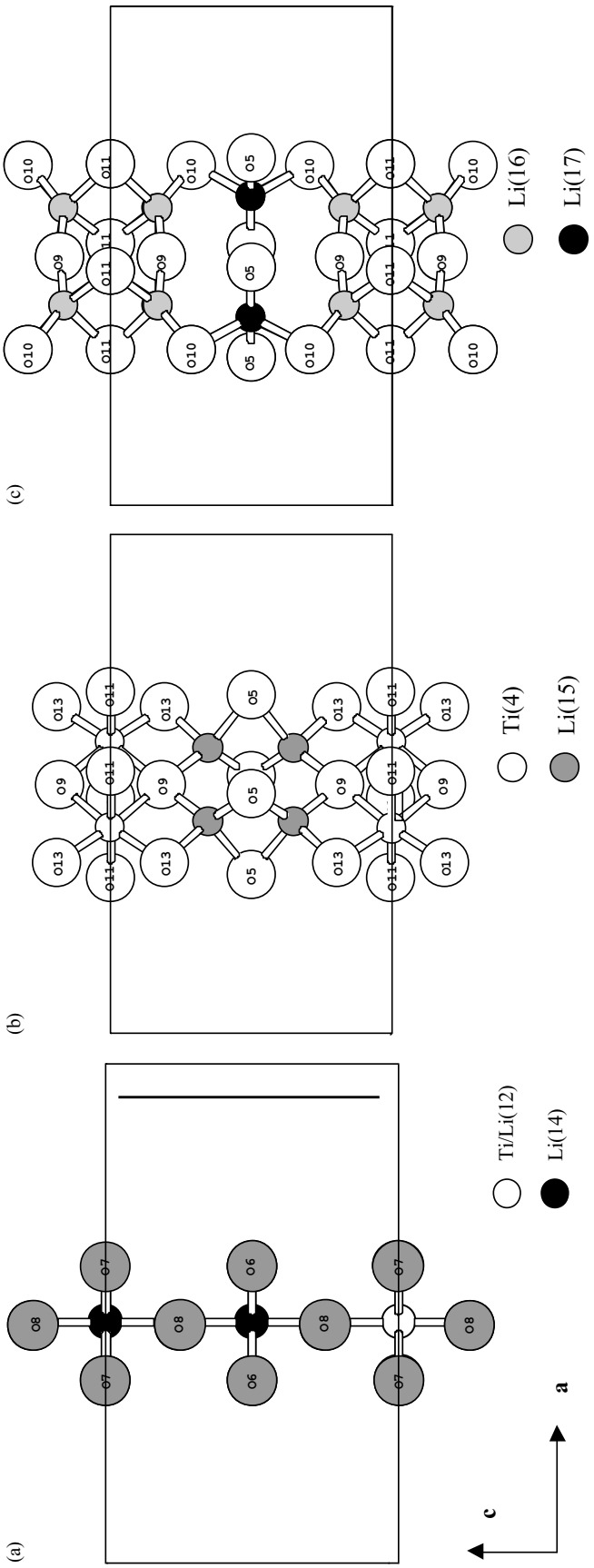

FIG. 6. Columns parallel to **c** of (a) perovskite structure, (b) fluorite segments containing four Li(15) in tetrahedral sites alternating with $Ti(4)O_6$ octahedra, and (c) fluorite segments containing four Li(16) in tetrahedral sites alternating with Li(17) in tetrahedral sites.

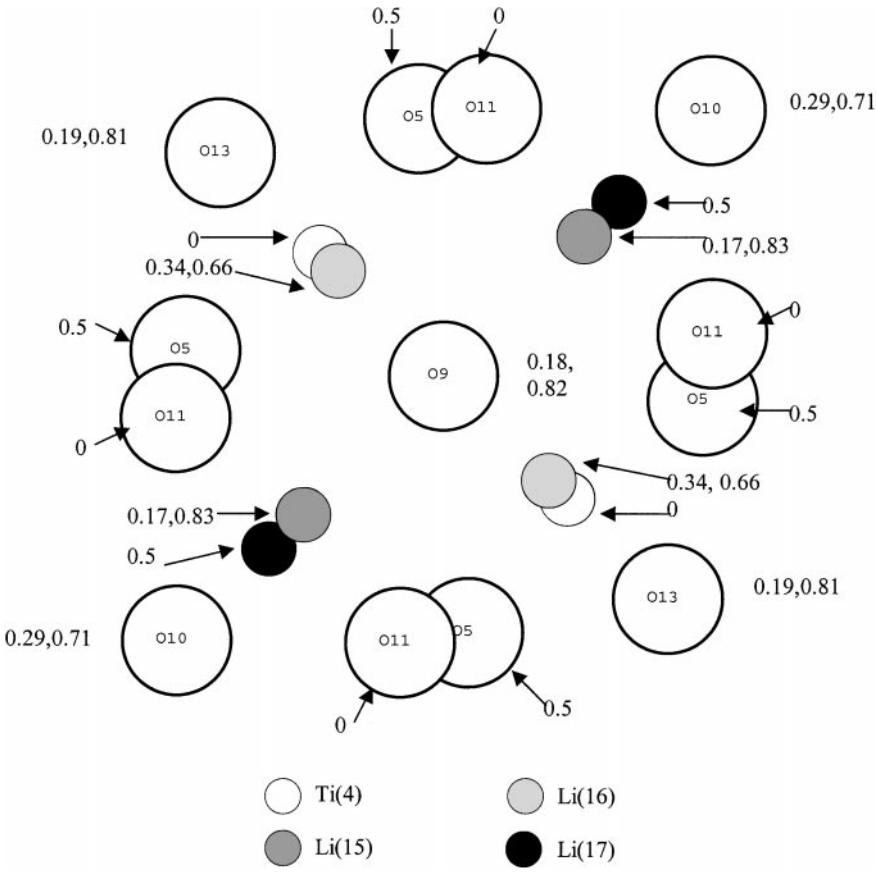

FIG. 7. Projection down **c** of the columns that show some similarity to the fluorite structure.

octahedra in a zig-zag arrangement may lead to a doubling of **c**. Indeed, tilting of the octahedra may also allow the axial Ti–O bonds to increase to give more acceptable values for octahedral coordination of Ti(12). Third, the partially occupied Li sites, Li(15) and Li(16), may be ordered.

To determine which mechanism is causing the presence of superlattice reflections is not possible from the present powder diffraction datasets. The intensities of the superlattice reflections may increase if the origin of the ordering is more pronounced at low temperatures. Hence, low-temperature studies of powder or single crystals may be useful. It is possible to have different ordering mechanisms or degrees of ordering in a sample of the same compound; this has been observed in single-crystal studies of Li_4SiO_4 (10).

From the SAED studies, which are essentially single-crystal diffraction studies, it appears that there are differences between some of the crystals, noted in the differences between diffraction patterns. Thus, some but not all of the crystals examined by SAED showed the presence of streaking along c*. The origin of the streaking is not understood, but could be due to partial order and/or formation of small ordered domains, or to the occurrence of stacking disorder in the subcell structure.

All three diffraction techniques were required to elucidate the subcell structure of $La_{24}Li_{20}Ti_5O_{56}$: SAED for unit cell and space group determination, XRD data as input to the direct methods program to locate the three La positions, and combined XRD and ND data to locate the missing atoms, using iterative partial Rietveld refinement and DFA. Solving structures from powder diffraction data is a relatively new technique and still in the development stages. The structure of $La_{24}Li_{20}Ti_5O_{56}$, with 57 positional and U_{iso} parameters, is probably one of the most complex yet to be solved by *ab initio* powder diffraction methods. The crystal structure of $La_{24}Li_{20}Ti_5O_{56}$ is not fully close-packed, cp. Nevertheless, the two sets of columns, individually, approximate to cp with fcc arrays of La, O in the perovskite-like columns and of O in the fluorite-related columns. Because the two sets of columns are rotated by 45 relative to each other, the structure does not develop a fully 3D *fcc* arrangement. The overall density is nevertheless comparable to that of a fully dense *cp* structure with 16.36 $Å^3$ per packing atom (La, O).

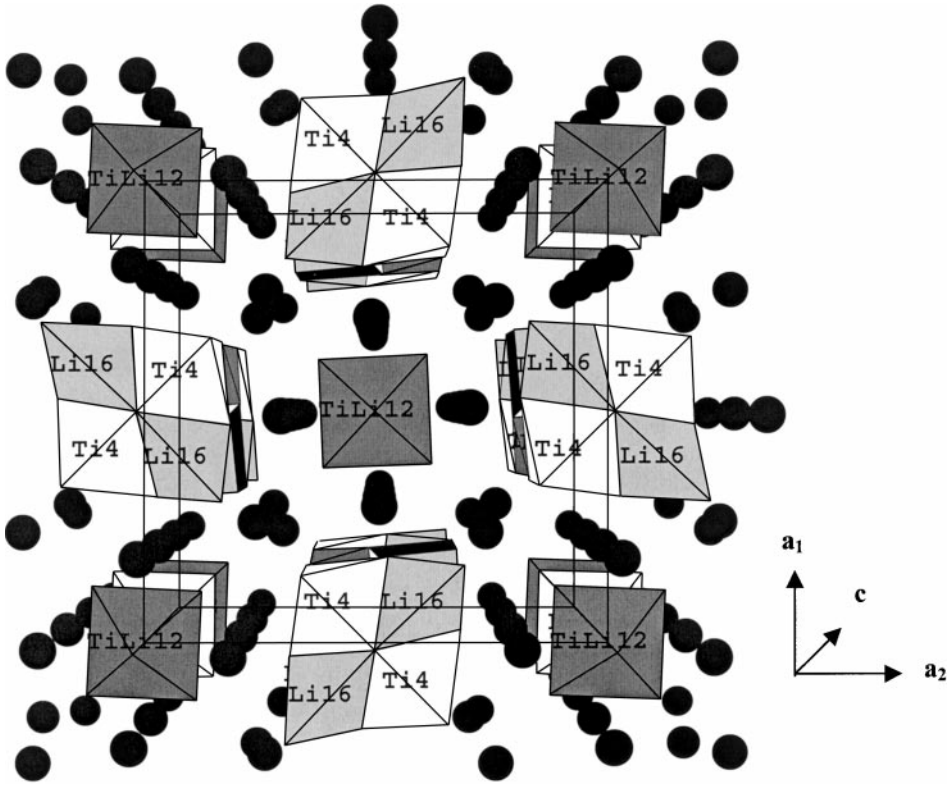

FIG. 8. Perspective view down [001] of $La_{24}Li_{20}Ti_5O_{56}$ with Ti and Li polyhedra indicated.

REFERENCES

1. Y. Inaguma, C. Liquan, M. Itoh, T. Nakamura, T. Uchida, H. Ikuta, and M. Wakihara, *Solid State Commun.* **86,** 689 (1993).
2. A. D. Robertson, S. Garcia-Martin, A. Coats, and A. R. West, *J. Mater. Chem.* **5,** 1405–1412 (1995).
3. C. A. Kirk, Ph. D. Thesis, University of Aberdeen, 2000.
4. C. A. Kirk, E. E. Lachowski, and A. R. West, *Chem. Commun.* 1437–1438 (2000).
5. F. Abbattista, D. Mazza, M. Vallino, and M. Gazzano, *J. Less Common Metals* **144,** 311–319 (1988).
6. A. Altomare, G. Cascarano, C. Giacvazzo, A. Guagliardi, M. C. Burla, G. Polodori, and M. Carmalli, *J. Appl. Cryst.* **27,** 435 (1994).
7. A. C. Larson and R. B. Von Dreele, Los Alamos Laboratory Report No. La-Ur-86-748, 1998.
8. R. Gunawardane, J. G. Fletcher, M. A. K. L. Dissanayake, R. A. Howie, and A. R. West, *J. Solid State Chem.* **112,** 70–72 (1994).
9. A. M. Coats, N. Hirose, J. Marr, and A. R. West, *J. Solid State Chem.* **126,** 105–107 (1996).
10. D. Tranqui, R. D. Shannon, H. Y. Chen, S. Iijima, and W. H. Baur, *Acta Crystallogr. B* **35,** 2479–2487 (1979).